THE JOURNAL OF PHYSICAL CHEMISTRY B
A JOURNAL OF THE AMERICAN CHEMICAL SOCIETY

pubs.acs.org/JPCB

Article

Permeability and Dynamics of a Monolayer are Mediated by ITO Support Surface-Modification

Homa Sadeghzadeh, Diana K. Nazario Torres, and G. J. Blanchard*

Cite This: *J. Phys. Chem. B* 2023, 127, 7785−7795

Read Online

ACCESS | Metrics & More | Article Recommendations | Supporting Information

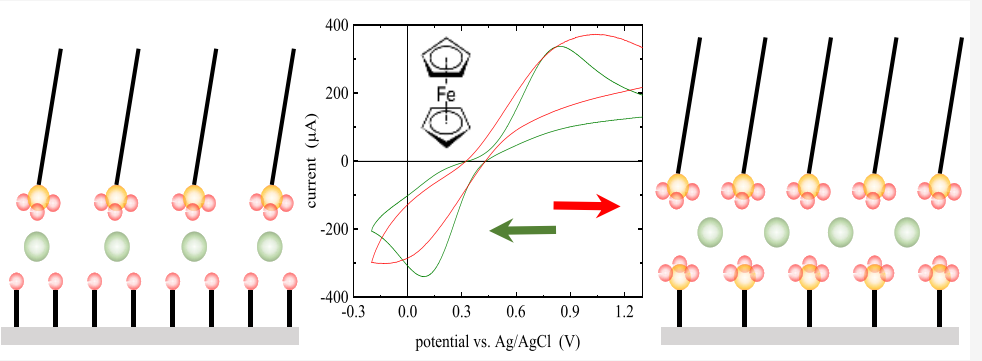

ABSTRACT: Indium tin oxide (ITO) has been extensively used as a transparent conductor. The surface chemistry of ITO is amenable to reactions similar to those used to modify silica, but a long-standing issue has been understanding the density and robustness of the ITO surface-modification. We report on the formation of chemically bound Cd^{2+}-complexed octadecylphosphonic acid (ODPA) monolayer formed on a Langmuir trough and deposited using Langmuir−Blodgett (LB) methodology onto an ITO surface, either in its native form or functionalized with phosphonate (RPO_3^{2-}). The organization of the Langmuir monolayer depends on the pH and presence of Cd^{2+} in the aqueous subphase on which it is formed and on the functionalization of the ITO surface. We probe the permeability of the resulting LB−support interface electrochemically and the motional freedom characteristic of chromophores contained within the monolayer using fluorescence recovery after photobleaching (FRAP). Our data demonstrate that without modification of the ITO surface the monolayer is significantly permeable by the electrophores used (ferrocene and Ru^{3+}), and surface modification to produce covalently bound phosphonate functionality results in a monolayer that is impermeable to the electrophores. FRAP studies reveal a relatively rigid monolayer aliphatic chain region for deposition on either native or modified ITO, suggesting direct Cd^{2+}−ITO interactions.

INTRODUCTION

Indium tin oxide (ITO) is a widely used semiconductor because of its combined properties of optical transparency in the visible region of the spectrum and its relatively high conductivity. We have used ITO as a support for interfacial monolayer growth and for control of surface charge in work with room temperature ionic liquids. In some instances, we have applied surface modification chemistry to facilitate either covalent or ionic bonding of molecules to the ITO surface. Indeed, there is rich literature on the surface modification of ITO.[1−17] Empirically, we have found that the chemical reactions that have been used to modify silica surfaces can also be used to modify ITO surfaces, but gaining a detailed understanding of the ITO surface remains to be achieved.

Silica and ITO are distinctly different surfaces, in terms of chemical functionality. Silica surfaces are known to possess silanol groups with a density of *ca.* 5 μmol/m^2, and with a pK_a for one subset of those groups of *ca.* 4.5. At neutral pH, the silica surface carries a net negative charge. ITO, in contrast, is known to exhibit a net positive surface charge for pH values below 6,[18] and surface hydroxyl functionality on ITO surfaces is seen only after oxygen plasma treatment.[1] Despite these clear differences, ITO that has not undergone oxygen plasma treatment reacts with $POCl_3$ in the presence of a Lewis base to produce a surface containing phosphonate functionalities.[19,20] Even though the surface reaction chemistry is similar for these two different surfaces, the question remains as to how the properties of the resulting interfaces differ. Making a direct electrochemical comparison between ITO and silica is not possible because ITO is conductive, while silica is a dielectric

Received: April 28, 2023
Revised: August 28, 2023
Published: September 1, 2023

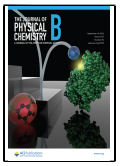

https://doi.org/10.1021/acs.jpcb.3c02803
J. Phys. Chem. B 2023, 127, 7785−7795

material. Much is known, however, about the silica surface, including that its morphology is extremely complex and the distribution of surface silanol groups is not homogeneous. Rather, the surface silica functionality is seen to exist in "islands" of *ca.* 15 nm diameter with narrow regions of lower silanol density between the islands.[21] Similar morphology has not been observed, to our knowledge, for ITO. The aim of this work is to evaluate the properties of surface monolayers deposited onto ITO, prior to and following its modification with $POCl_3$ in the presence of a Lewis base to produce surface phosphonate functionality. The amphiphile used to form the monolayers is octadecyl phosphonic acid (ODPA), performed on a Langmuir trough and deposited using the Langmuir−Blodgett (LB) technique.[22−24] We construct a series of monolayer structures deposited onto native and modified silica and ITO, and in the presence and absence of Cd^{2+} in the aqueous subphase of the Langmuir trough. The interfaces were evaluated optically (ITO and silica) and electrochemically (ITO only). To gauge the permeability of the interfaces, we used ferrocene and Ru^{3+} to determine the extent to which the monolayers on ITO were penetrable by the electrophores. Our findings revealed that when a Cd^{2+}-bisphosphonate linkage was formed to bind the ODPA monolayer to the modified surface, Faradaic current was not observed for either electrophore. Further investigation of the extent of organization within the resulting monolayer interface was performed by incorporating perylene into the Langmuir monolayer during formation and evaluating the diffusional properties of the chromophore within the interface following LB deposition onto the modified ITO interface. Our data demonstrate that the aliphatic region of the interface exists as a comparatively viscous fluid, with chromophore diffusional motion being mediated by the interchain interactions, organization within the monolayer, and the mobility of the amphiphile monolayer constituents.

METHODS

Materials. Octadecyl phosphonic acid (ODPA), $CdCl_2$, $RuCl_3$, ferrocene (Fc), tetrabutylammonium hexafluorophosphate ($TBAPF_6$), acetonitrile, 2,4,6-collidine, $POCl_3$, and perylene were obtained from Sigma-Aldrich in their highest purity forms and used without further purification. Acetonitrile was dried over a molecular sieve prior to use. All ODPA solutions used for monolayer deposition were prepared at a concentration of 1 mg/mL in tetrahydrofuran (THF). For the growth of Cd^{2+}−ODPA monolayers, $CdCl_2$ was dissolved in Milli-Q water at the desired concentration to constitute the aqueous subphase. Water (18 MΩ) from a Milli-Q filtration system was used for the subphase in all Langmuir−Blodgett monolayer growth and deposition cycles. Subphase pH was controlled with HCl (1 M, CCI, Inc.).

Monolayer Deposition. Films were deposited on glass microscope cover slides that were coated with indium tin oxide (ITO) (#1, 22 mm × 22 mm, Alkali Scientific, Inc.). The resistance of the ITO films is 10 Ω/square. All glass substrates were cleaned by immersion in piranha solution ($1H_2O_2$:$3H_2SO_4$; ***caution:*** *strong oxidizer!*) for 10−15 and 15 min, followed by rinsing with Milli-Q water until the pH of the rinse was *ca.* 7. Substrates were stored in Milli-Q water to minimize adventitious contamination by airborne organic compounds. For cleaning the ITO-coated supports, a beaker is filled with Milli Q water and detergent (Fisher Sparklin 1), and then the support is added and sonicated for 10 min. The beaker is then rinsed with Milli Q water until the detergent is removed, and then filled with only Milli Q water and sonicated for 10 min. Water is then decanted, and the beaker is filled with 2-propanol and sonicated for 15 min. The ITO-coated cover slide is then dried under a flowing stream of $N_2(g)$ to remove 2-propanol. The cleaned cover slide is then submersed (vertically) into the Langmuir trough.

Phosphonation Reaction. ITO was modified by using a procedure reported previously.[20] The clean surface was immediately phosphonated by immersion in 100 mM $POCl_3$ and 100 mM 2,4,6-collidine in dry acetonitrile for 1 h, and then rinsed with anhydrous acetonitrile. Then the modified surface was stored under Milli-Q water.

Langmuir Film Formation. All Langmuir monolayers were formed by using a Langmuir trough (KN 2003, KSV Nima, Biolin Scientific, Gothenburg, Sweden) equipped with a Brewster angle microscope (BAM) attachment (UltraBAM, Accurion, Göttingen, Germany) and a platinum Wilhelmy plate balance for measuring surface pressure. The aqueous subphase of the trough is temperature controlled, 20.0 ± 0.1 °C. The pH of the subphase was measured using a pH meter with the pH being controlled through the addition of HCl or NaOH. The ITO/glass substrate is immersed in the trough prior to application of the monolayer deposition solution. Approximately 1 h was allotted for subphase equilibration, and then 70 μL of the ODPA in THF spreading solution were deposited beneath the subphase surface by using a syringe, with care taken to ensure the initial surface pressure did not exceed 0.5 mN/m. Following a 20 min solvent evaporation period, monolayer compression was initiated at a barrier speed of 5 mm/min. For monolayer deposition, barrier compression stopped when the surface pressure reached the desired pressure of 35 mN/m depending on the experiment. The barrier position was placed at the desired surface pressure for *ca.* 10−15 min to allow for monolayer equilibration. Film deposition was performed by the vertical removal of the immersed substrate from the subphase at a rate of 2 mm/min. Following complete removal from the subphase, the substrate was maintained above the trough for *ca.* 30 min to allow any residual water to evaporate. All experiments were controlled by using KSV NIMA LB software (version 2.2, Biolin Scientific). The Brewster angle microscope was controlled with the UltraBAM 1.1.2 software (Accurion), and the angle of incidence was set to 53.2° (θ_B for H_2O). Film formation images were acquired by using Accurion Image 1.1.3 software (Accurion).

Cyclic Voltammetry Studies. A 25 mL solution of $TBAPF_6$ (0.1 M) in acetonitrile was prepared, and that solution was used to prepare a 1 mM solution of ferrocene or 1 mM of Ru^{3+}. All of the measurements were done using $TBAPF_6$ as an electrolyte. The working electrode is 1.5 cm ITO, the reference electrode is Ag/AgCl 1 M from CH Instruments, and the counter electrode is platinum wire. The scan rate was 100 mV/s, and the windows varies based on the solution of studies.

Fluorescence Recovery after Photobleaching (FRAP). FRAP measurements are made using a Nikon Eclipse Ti-E inverted microscope equipped with a confocal scanning system (Nikon Ti-S-CON). A 20× objective lens was used for all experiments. For perylene, the 405 nm diode laser was used for excitation (Nikon C2-DU3, 400−700 nm). For all measurements, the initial image intensity was recorded for 1 min and bleached for 30 s, and the recovery was monitored for a

https://doi.org/10.1021/acs.jpcb.3c02803
J. Phys. Chem. B 2023, 127, 7785−7795

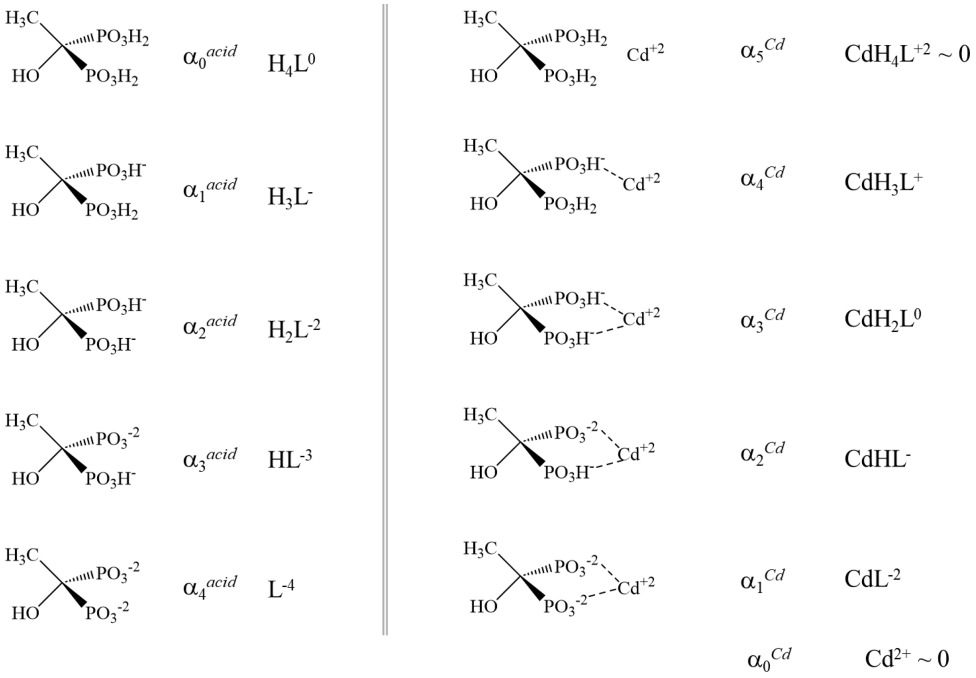

Figure 1. Structures of HEDP as a function of protonation (left) and complexation with Cd^{2+} (right).

minimum of 3 min. At least five spots across each plate were measured in this manner.

RESULTS AND DISCUSSION

Our long-term interest in complexed monolayer systems lies in the ability to modify the organization and fluid behavior of the monolayer reversibly through control over the oxidation state of the metal ion used in the formation of the monolayer. In the work reported here, we focus on the formation of metal-phosphonate and metal-bisphosphonate monolayers with Cd^{2+} as the metal ion. A precursor to being able to control monolayer morphology reversibly is that the organization, complexation chemistry, and consequent properties of the monolayers are well understood. The use of Cd^{2+} offers an opportunity to evaluate the role of ITO surface modification on the properties of the resulting monolayers. We consider first the details of monolayer formation on the Langmuir trough as a function of aqueous subphase pH. We then probe the permeability of LB monolayers deposited on unreacted ITO and on phosphonated ITO using two electrochemical probes: Ru^{3+} and ferrocene (Fc). With this information in place, we then consider the fluid properties of the monolayer on both native and modified ITO supports.

Before considering the relevant equilibria, it is instructive to consider the structural framework in which this work exists. The Talham group has reported previously on ODPA multilayers where a variety of divalent and trivalent metal ions have been incorporated.[25−27] They found that the complexation of the metal ions within the bisphosphonate multilayers was structurally the same as that for the corresponding bulk metal bisphosphonate. This structural information serves as a guide for the structures expected in this work. Their work also indicated the pH ranges in which the ODPA-metal ion monolayers were formed. This important experimental consideration is the result of the competitive equilibria that operate during the formation of the Langmuir monolayers and which we consider in detail below.

Relevant Equilibria. The amphiphile used in the formation of the Langmuir monolayers is octadecylphosphonic acid, ODPA, and we use Cd^{2+} to form complexes with the monolayer at the interface. Modeling the complexation requires consideration of the extent to which the phosphonic acid head groups are dissociated and the extent to which the Cd^{2+} forms complexes with partially and fully dissociated phosphonic acid headgroups. While there is limited direct information on the formation constants for this specific system, there is a model compound that can be used to approximate the complexation(s) of interest. The model system is hydroxyethyldiphosphonic acid (HEDP, Figure 1). There exist data for the complexation of HEDP in its several deprotonated states. While the structure of HEDP is not the same as that expected for the complexed monolayer, it does possess a structure that is closer to that of a plane of phosphonates than bulk solution phase complexation of Cd^{2+}. With that caveat in mind, we consider the extent of protonation of HEDP as a function of pH as well as the extent of complexation of the various forms of HEDP with Cd^{2+}. For the purposes of this discussion, we designate the various forms of HEDP as H_4L^0, H_3L^-, H_2L^{-2}, HL^{-3}, and L^{-4} (eq 1),

$$H_4L^0 \overset{k_{a1}}{\rightleftharpoons} H_3L^- + H^+ \overset{k_{a2}}{\rightleftharpoons} H_2L^{-2} + H^+ \overset{k_{a3}}{\rightleftharpoons} HL^{-3} + H^+ \overset{k_{a4}}{\rightleftharpoons} L^{-4} + H^+ \quad (1)$$

and Cd^{2+} can form complexes with each form of HEDP (eq 2).

$$Cd^{2+} + L^{-4} \overset{k_0}{\rightleftharpoons} CdL^{-2} + H^+ \overset{k_1}{\rightleftharpoons} CdHL^- + H^+ \overset{k_2}{\rightleftharpoons} CdH_2L^0 + H^+ \overset{k_3}{\rightleftharpoons} CdH_3L^+ \quad (2)$$

Based on these pH-dependent reactions, we can calculate the α-fractions for each form of HEDP (eqs S1−S7) and for each Cd−HEDP complex (eqs S8−S14). The α-fraction plots for the HEDP species and Cd−L complex species are shown in Figure 2a and 2b, respectively. In these calculations we have

https://doi.org/10.1021/acs.jpcb.3c02803
J. Phys. Chem. B 2023, 127, 7785−7795

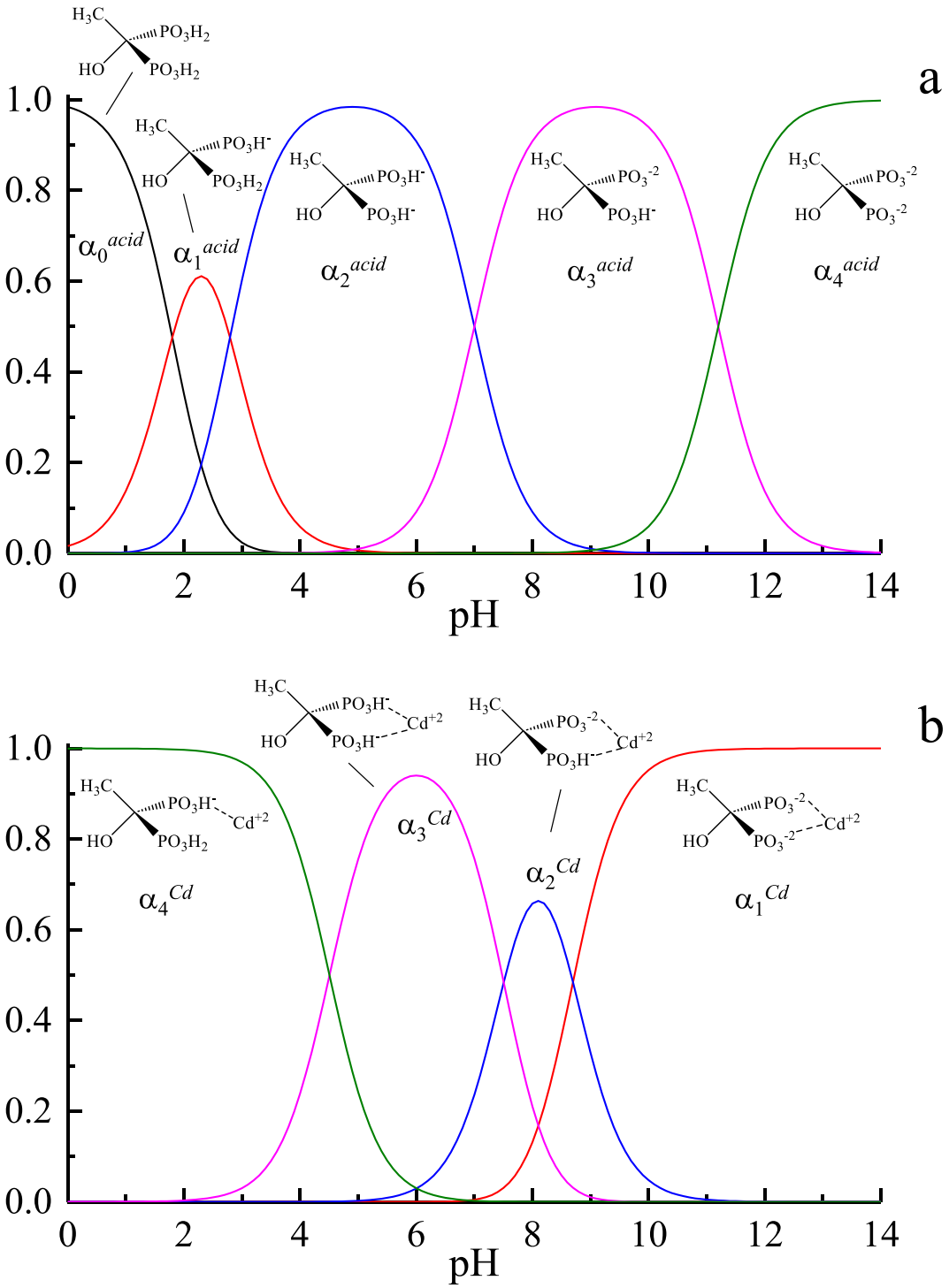

Figure 2. (a) Acid α-fractions for HEDP as a function of pH and (b) complexation α-fractions for Cd-HEDP complexation as a function of pH.

not included a term for CdH_4L^{2+} because it is not seen in the LB and BAM data (*vide infra*) to contribute and due to the absence of information available on the formation constant for this species. The constants k_i used in the α-fraction calculations are given in Table S1. With this information in mind, we consider the pH dependence of the LB monolayer formation.

Langmuir Monolayer Formation and LB Deposition. We have formed ODPA Langmuir monolayers and have examined their organization through their pressure−area (Π−A) isotherms and Brewster angle microscopy (BAM) images as a function of aqueous subphase pH and $[Cd^{2+}]$. We present these data in Figure 4. The isotherm and microscopy data provide complementary information about the packing and morphology of the monolayers. The data reveal a clear pH-dependent trend, which can be understood in the context of the α-fraction plots shown in Figure 2 and the corresponding schematics in Figure 3. These results are consistent with other reports on ODPA mono- and multilayer formation using Langmuir films.[25−27]

The isotherm data (Figure 4) show a progression in functional form that varies in a regular manner with pH. At pH 5.9, the isotherm has liquid-analogous behavior over the entire

https://doi.org/10.1021/acs.jpcb.3c02803
J. Phys. Chem. B 2023, 127, 7785−7795

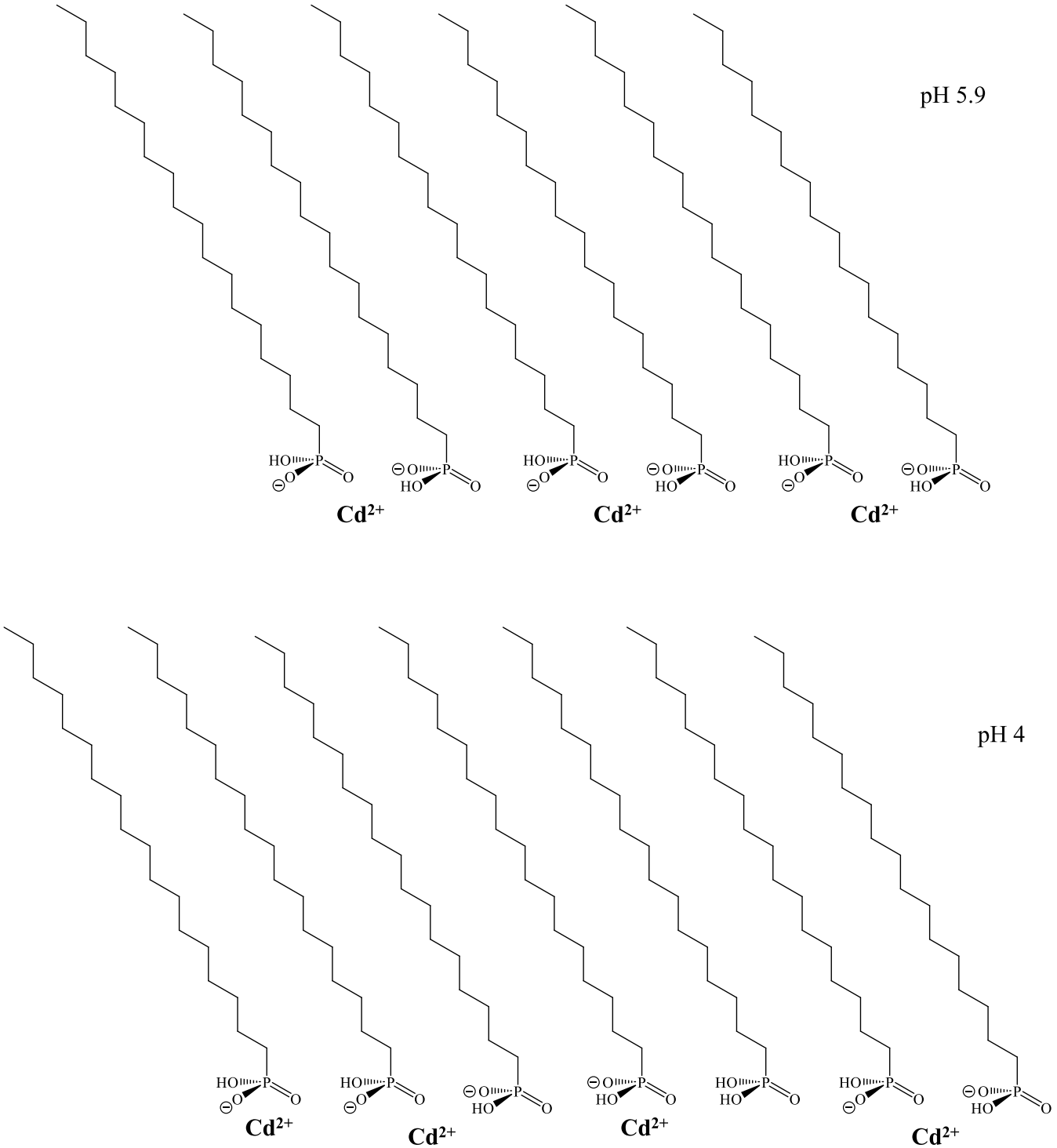

Figure 3. Schematic of ODPA Langmuir monolayer coordination of Cd^{2+} in the vicinity of pH 5.9 (top) and 4.0 (bottom). The schematic is intended for illustrative purposes only and is not a calculated or measured result.

pressure range, with a decrease in slope at higher pressures. The high-pressure region of this isotherm may reflect compression of individual domains. In the pH range of 4.3 to 4.0 there is a progression from predominantly liquid-analogous behavior (pH 4.3) to something closer to liquid-condensed (pH 4.2−4.1), to the classic gas-to-liquid-to-solid isotherm with monolayer collapse with decreasing mean molecular area (pH 4.0). We attribute this trend to changes in the extent of complexation between ODPA and Cd^{2+}. The extent of protonation and complexation of the ODPA headgroup can be seen most easily by examination of the α-fraction plot (Figure 2), which shows that, at pH 5.9, the dominant form of the complex is between two monodeprotonated ODPA molecules and one Cd^{2+} ion. In the vicinity of pH 4, there are approximately equal amounts of complexation between two monodeprotonated ODPA molecules and Cd^{2+}, and one monodeprotonated ODPA molecule and Cd^{2+}. As the ODPA:Cd^{2+} stoichiometry decreases based on headgroup

https://doi.org/10.1021/acs.jpcb.3c02803
J. Phys. Chem. B 2023, 127, 7785−7795

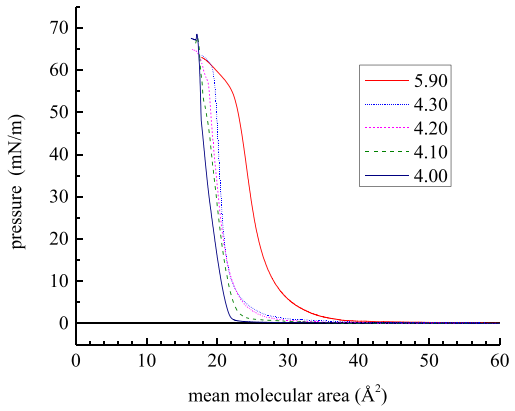

Figure 4. Pressure−area (π−A) isotherms of Cd-ODPA Langmuir−Blodgett monolayers for three pH values of 0.1 mM of $CdCl_2$ subphase. pH Values for each isotherm are as indicated in the legend.

charge, there is more opportunity for amphiphile interactions in the aliphatic chain region to contribute to the monolayer structure, and at high pH values, such as 5.9, the Cd^{2+} interaction with two phosphonate functionalities dominates the spacing of the amphiphiles within the monolayer. The Brewster angle microscopy data (Figure 5) are helpful in

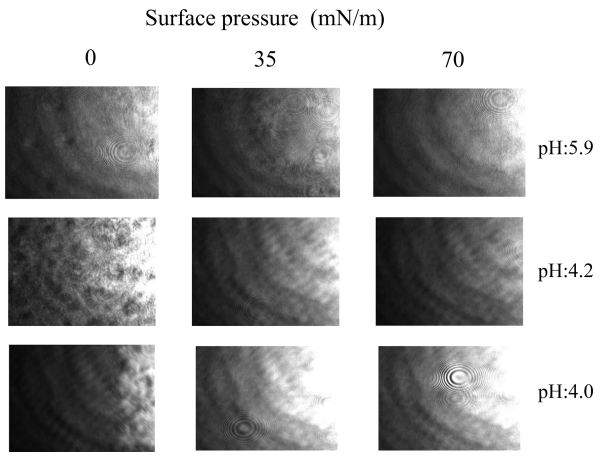

Figure 5. Brewster angle microscopy images of the Cd-ODPA monolayers corresponding to three different pressures and at three pH values. The corresponding π−A isotherms for these images are shown in Figure 4. BAM data for pH 4.1 and 4.3 are shown in Figure S1.

understanding nascent organization in these monolayers, especially at a low pressure. Under gas phase conditions (0 mN/m) there appear to be aggregate structures (dark regions) that are likely formed based on metal ion coordination. At the higher surface pressures, the monolayers all appear to be similar in morphology, and this is not a surprising result, because any organization in these structures is expected to be over characteristic length scales below the resolution of the BAM microscope.

With the Langmuir monolayer formation established, the next stage in the formation of the interfaces of interest is to deposit the monolayers onto solid supports by vertical withdrawal of the support from the Langmuir trough. We consider the properties of the ODPA monolayers formed under several different conditions, where the ITO-coated support either is in its native state or reacted with $POCl_3$ and H_2O to add surface phosphonate functionalities. Comparing the properties of ODPA monolayers complexed with Cd^{2+} present in the aqueous subphase deposited on native and phosphonated surfaces will provide insight into the role that the Cd^{2+}-bisphosphonate linkage plays in determining monolayer properties. We expect that the nature of the interfacial bond will be substantially different for the two surface modifications and have interrogated the differences in these monolayer systems both electrochemically and optically.

Electrochemical Characterization. The issues of extent of coverage and defect density in monolayers can be examined electrochemically. We have used two electrochemical probes, Ru^{3+} and ferrocene (Fc), to evaluate their access to the ITO electrode surface. These two electrochemical probes were chosen because of their well-known electrochemical properties. All electrochemical experiments were performed in acetonitrile, and 0.1 M $TBAPF_6$ was used as the electrolyte. Before considering the cyclic voltammetry (CV) of Ru^{3+} or Fc, we performed CV measurements on 0.1 M $TBAPF_6$ in ACN (Figure S2). The CVs exhibited Faradaic current only for solvent reduction for all samples studied. The native ITO electrodes produced the highest currents, with the Cd^{2+}-ODPA monolayer on native ITO showing an attenuated solvent reduction wave. The Cd^{2+}-ODPA on phosphonated ITO exhibited a very low non-Faradaic current, consistent with effective blockage of the electrode surface by the bound monolayer. No monolayer or electrode constituent produced a Faradaic response in this potential window. We next considered the CV data for Ru^{3+} and Fc.

The CV data for Ru^{3+} are shown in Figure 6 for the same electrode surfaces used for the $TBAPF_6$ data. The CV of $Ru^{2+/3+}$ has been examined extensively and is known to exhibit a number of redox waves associated with different Ru-oxide species.[28,29] The data shown in Figure 6 are characteristic of reduction and oxidation processes, and we assign the reduction feature at +0.40 V to the reduction of Ru^{2+} and the reduction wave at +0.71 V to the reduction of Ru^{3+}. We note that it is more typical to use Ru complexes with nitrogen heterocycles as redox probes. Our motivation for the use of Ru^{3+} in ACN was to use a somewhat less bulky electrophore. We have not characterized the complexation of Ru by ACN, but there is precedent for coordination of these species.[30] The data show that the largest currents are seen for the native ITO and phosphonated ITO electrodes. The Cd^{2+}-ODPA monolayer on native ITO produces somewhat lower current, demonstrating that presence of the unbound monolayer does not prevent access of Ru^{3+} to the ITO electrode surface. The phosphonated ITO electrode with a Cd^{2+}-ODPA monolayer produces a lower current, suggesting significant coverage of the ITO surface by the surface modification. The deposition of a Cd^{2+}-ODPA monolayer on phosphonated ITO reduces the current to the point where a Ru^{3+} reduction wave is barely discernible at a 100 mV/s scan rate, but is seen clearly for a 500 mV/s scan rate. This result is due to either depletion of Ru^{3+} at the lower scan rate or disruption of the monolayer organization by the higher scan rates. The scan rate dependence of these data (Figure S3) suggest the latter explanation is operative.

The CV data for Fc are shown in Figure 7. Fc is known to be an ideal reversible redox couple under most conditions, but the change in oxidation and reduction potentials seen as a function of ITO surface modification point to either a difference between the oxidized (charged) form and the reduced (neutral) form in terms of access to the electrode surface.

https://doi.org/10.1021/acs.jpcb.3c02803
J. Phys. Chem. B 2023, 127, 7785−7795

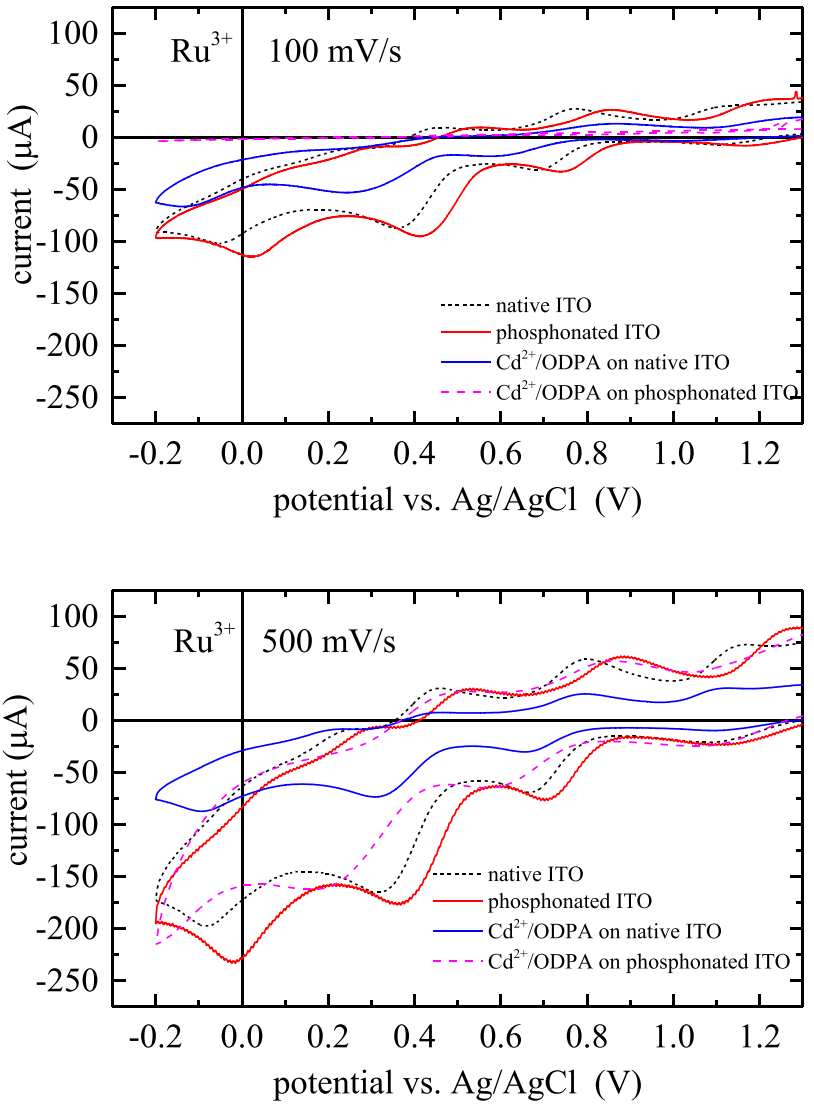

Figure 6. Cyclic voltammogram of the bare ITO (black), phosphonated bare ITO (red), Cd-ODPA monolayer on ITO (blue), Cd-ODPA on phosphonated ITO (magenta) in 1 mM $RuCl_3$ (electrolyte: 0.1 M $TBAPF_6$ solution). Top: scan rate = 100 mV/s. Bottom: scan rate = 500 mV/s.

Irreversibility has been seen before for Fc, and it has been understood in terms of the reaction of Fc with Cl^-,[31−33] and that is one possible contribution to the observed data. The presence of Cl^- in our monolayers could be explained by the way the pH is controlled in the subphase with HCl or the phosphonation reaction of ITO involves the elimination of Cl^- following the initial reaction. For the Cd^{2+}-ODPA monolayers, Cd can associate with Cl^- until complexation, leaving displaced Cl^- present in the monolayer, presumably in the region of the Cd-bisphosphonate functionality. Despite these possibilities, we have not observed Cl^- in the XPS data on any of our support surfaces (data not shown), and the variation seen in the data is most likely due to surface modification of the ITO surface. The Fc CV data indicate that it is capable of penetrating the monolayer to an extent. For a scan rate of 100 mV/s, Fc Faradaic current is negligible, but it is seen clearly for a 500 mV/s scan rate. The change in peak separation with scan rate suggests relatively slow electron transfer at the electrode, which could be caused either by surface modification or, possibly, the ITO surface itself. Further investigation will be required to understand the dominant factor. As for the Ru^{3+} data (Figure 6), these results could be accounted for by either Fc depletion at low scan rates or monolayer disruption at higher scan rates (Figure S4). The data appear to be more consistent with the latter explanation.

Of particular relevance to this work is the effective blockage of the ITO electrode for the Cd^{2+}-ODPA monolayer deposited on the phosphonated ITO surface. This finding is consistent with strong monolayer bonding through the Cd-bisphosphonate functionality. The electrochemical data, taken collectively, point to the deposition of a Cd^{2+}-ODPA monolayer on native ITO not being held in place by any substantial forces, and this is not surprising. The deposition of the Cd^{2+}-ODPA monolayer on the phosphonated ITO surface results in a relatively complete and robust coverage of the surface. Divalent metal ions are thought to form bisphosphonate complexes that are substantially more labile than those seen for Zr^{4+} or Hf^{4+},[34−36] and in most cases M^{2+}-bisphosphonates have been seen to be unstable in aqueous environments.[37−40] Our findings, especially the effective blocking of access to the ITO electrode by the Cd^{2+}-ODPA monolayer on phosphonated ITO, suggest that the monolayer is sufficiently fluid to "heal" defects in the monolayer.

https://doi.org/10.1021/acs.jpcb.3c02803
J. Phys. Chem. B 2023, 127, 7785−7795

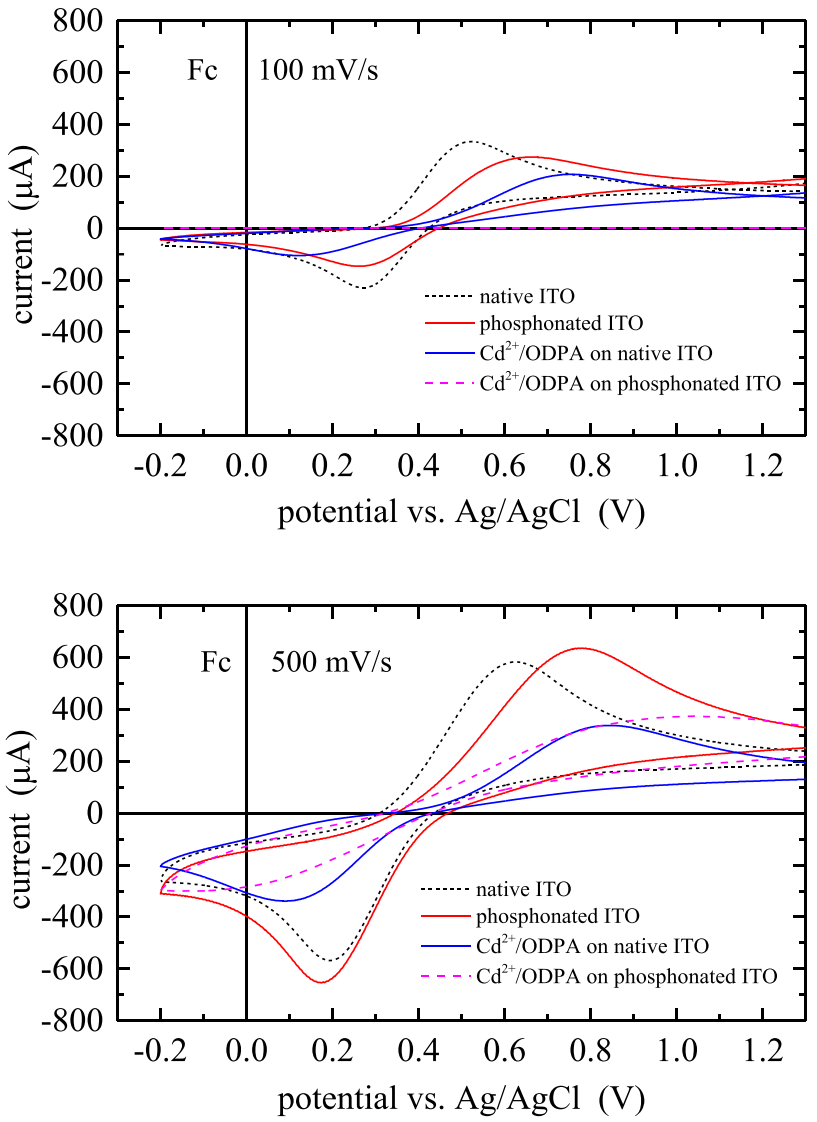

Figure 7. Cyclic voltammogram of the bare ITO (black), phosphonated bare ITO (red), Cd-ODPA monolayer on ITO (blue), Cd-ODPA on phosphonated ITO (magenta) in 1 mM Ferrocene (electrolyte: 0.1 M $TBAPF_6$ solution). Top: scan rate = 100 mV/s. Bottom: scan rate = 500 mV/s.

Chromophore Dynamics within the Monolayers. To gauge the fluid nature of the Cd^{2+}-ODPA monolayer, we have performed fluorescence recovery after photobleaching (FRAP) experiments using perylene as a chromophore incorporated into the monolayer during its formation. FRAP measurements are used to characterize the diffusion constant of the perylene chromophore. The interpretation of FRAP data depends on the nature of the interactions between the chromophore and its environment, and for the system we consider here, there is no opportunity for the chromophore to bond to either the monolayer constituents or the support surface. Using the free-diffusion model, we fit the FRAP recovery curves (Figures S5–S7) to established models.[41,42] The translational diffusion constant is related to the thermal energy in the system (k_BT), the size of the diffusing species (r), and the viscosity of the monolayer medium (η). We extract D_T from the FRAP data, and from that information we determine η using eq 3,

$$\eta = \frac{k_B T}{6\pi r D_T} \tag{3}$$

where T = 293 K and the hydrodynamic volume of perylene is 225 Å^3, yielding a value of r = 3.8 Å. We summarize the values for D_T and η in Table 1 as a function of support surface chemistry and Langmuir through subphase pH (subphase $[Cd^{2+}]$ = 0.1 mM). There are several pieces of useful information contained in these data. Considering the values of D_T extracted from the experimental FRAP data, there is a clear difference in the values for the LB monolayer deposited on native glass, phosphonated glass, and ITO. We understand that the interaction of the ODPA monolayer with the glass support will be weaker than its interactions with either native or phosphonated ITO, and this difference would lead to a higher mobility of the amphiphiles and consequently a larger (and more pH-sensitive) measured diffusion constant. The reason that we include this information is that, by comparing FRAP results on glass and phosphonated glass with those on ITO, we are able to evaluate the contributions of diffusion from the mobility of the chromophore through the monolayer and from the mobility of the amphiphiles which comprise the monolayer. The value of D_T for perylene, which is contained in

https://doi.org/10.1021/acs.jpcb.3c02803
J. Phys. Chem. B 2023, 127, 7785−7795

Table 1. Values of D_T and η for the LB-Monolayer Derived from Experimental FRAP Data as a Function of Support Surface[a]

Support Surface	Diffusion constant D_T ($\mu m^2/s$)	Viscosity η (cP)
Native glass pH: 4.1	0.65 ± 0.03	870 ± 40
Native glass pH: 4.3	0.86 ± 0.29	710 ± 240
Native glass pH: 5	0.76 ± 0.05	750 ± 50
Phosphonated glass pH: 4.1	0.78 ± 0.25	770 ± 260
Phosphonated glass pH: 4.3	0.28 ± 0.09	2120 ± 690
Phosphonated glass pH: 5.9	0.25 ± 0.04	2310 ± 390
Native ITO pH: 4.2	0.19 ± 0.01	3080 ± 10
Phosphonated ITO pH: 4.2	0.18 ± 0.02	3160 ± 260

[a]For all measurements reported in this Table, $[Cd^{2+}]$ = 0.1 mM in the Langmuir through aqueous subphase.

the aliphatic chain region of the monolayer, is relatively high and pH-independent for the monolayer deposited on a glass support. When the LB monolayer is deposited on phosphonated glass, D_T for perylene is seen to be the same as that on glass at pH 4.1, but for monolayers deposited from subphases with pH 4.3 and 5.9, the measured value of D_T for perylene is smaller by a factor of *ca.* 3. We understand these values as indicating that the measured diffusion of the embedded perylene chromophore is mediated by both the ability of the chromophore to move within the nonpolar region of the monolayer and also the strength of interactions between the amphiphile monolayer and the support. In other words, it is the mobility of both the chromophore and amphiphile that contributes to the observed D_T for the native glass support and on the phosphonated support at pH 4.1. For pH values of 4.3 and 5.9, D_T for perylene becomes smaller because the mobility of the amphiphiles that comprise the monolayer has been greatly diminished by the formation of a Cd^{2+}-bisphosphonate linkage. Interestingly, the values for perylene D_T on native ITO and phosphonated ITO are the same to within the experimental uncertainty and are reflective of the amphiphiles exhibiting very limited mobility. These data imply that the Cd^{2+} is coordinating strongly to surface functionality on both the native and modified ITO supports. For the native ITO support, it is not clear what the nature of the coordination is, and this question remains to be investigated more thoroughly.

It is instructive to view these results from the perspective of the extracted viscosity values (Table 1). On native glass at all pH values examined and in phosphonated glass at pH 4.1, the apparent viscosity of the LB monolayer is seen to be *ca.* 750 cP. For the phosphonated glass supports at pH values of 4.3 and 5.9, the monolayer viscosity is *ca.* 2200 cP, and for both the native and phosphonated ITO surfaces, we recover a monolayer viscosity of *ca.* 3100 cP. By way of comparison, the viscosity of glycerol is *ca.* 1400 cP at room temperature. The measured perylene diffusion constants (and thus the calculated viscosities) depend on the mobility of both the chromophore and the amphiphiles that form the monolayer.

It is important to compare the results of the electrochemical characterization to those of the FRAP characterization. The electrochemical data for both electrophores (Figures 6, 7) show that the Cd^{2+}-ODPA monolayer on native ITO produces a Faradaic current higher than that for the Cd^{2+}-ODPA monolayer on the phosphonated ITO support. These data demonstrate more ready access to the ITO support (electrode) for the native ITO support, but the FRAP data produce identical FRAP results with small D_T for perylene in the amphiphile aliphatic chain region. Taken collectively, these data suggest a bonding interaction between the native ITO surface functionalities and Cd^{2+} that renders the amphiphile immobile to an extent similar to that seen for the same monolayer bonded to the phosphonated ITO support. The difference between the two monolayers may lie with the density of the monolayer coverage, although there are many potential structural issues related to the surface modification of ITO that complicate efforts to reconcile the CV and FRAP results. For the native ITO support, there appears to be more access to the ITO electrode than for the phosphonated ITO support. Perylene diffusion senses the deposited monolayer regions but not the extent of monolayer coverage on the support, while the electrochemical data sense the extent of monolayer coverage.

CONCLUSIONS

We have demonstrated control over the pressure−area isotherms for ODPA Langmuir monolayers through the pH and $[Cd^{2+}]$ of the aqueous subphase, and we understand the distribution of species contained in the resulting Cd^{2+}-complexed monolayer through the a-fractions of the multiple species present in this system. BAM data of these monolayers support the importance of Cd^{2+} complexation on the formation of the Langmuir monolayer. When these monolayers are deposited on silica and ITO supports, the extent and nature of the surface coverage are seen to depend on whether the monolayers are deposited on native phosphonated supports and whether Cd^{2+} is absent or present in the deposited monolayer assemblies. Interestingly, comparison of the electrochemical characterization of the monolayers deposited on the ITO supports shows that the phosphonated ITO support produces monolayers that provide very limited access to the ITO electrode, while deposition of the same monolayer on the native ITO support leads to greater access to the ITO electrode. FRAP data for perylene contained in the aliphatic chain regions of these same monolayers show the aliphatic chain regions of the monolayers to be essentially identical, suggesting a strong bonding of the amphiphiles to the ITO surface through Cd^{2+}. The specific functionalities to which the Cd^{2+} binds on the native ITO surface remain to be identified, but these data demonstrate chemical control over monolayer properties. It is thus likely that we will be able to establish electrochemical control over monolayer morphology through the oxidation state of the metal ion used.

ASSOCIATED CONTENT

Supporting Information

The Supporting Information is available free of charge at https://pubs.acs.org/doi/10.1021/acs.jpcb.3c02803.

Equations for the H^+ and Cd^{2+} α-fractions used in the calculations shown in Figures 2a and 2b, list of the constants used in the α-fraction calculations, additional BAM images of Langmuir monolayer formation, Cyclic voltammograms of bare ITO, phosphonated ITO, Cd-ODPA monolayer on ITO and Cd-ODPA on phosphonated ITO at 100 mV/s scan rate and Ru^{3+} and Fc in ACN at interfaces as a function of scan rate, FRAP data (intensity vs time). (PDF)

https://doi.org/10.1021/acs.jpcb.3c02803
J. Phys. Chem. B 2023, 127, 7785−7795

AUTHOR INFORMATION

Corresponding Author

G. J. Blanchard − *Michigan State University, Department of Chemistry, East Lansing, Michigan 48824, United States*; Phone: +1 517 353 1105; Email: blanchard@chemistry.msu.edu

Authors

Homa Sadeghzadeh − *Michigan State University, Department of Chemistry, East Lansing, Michigan 48824, United States*

Diana K. Nazario Torres − *Michigan State University, Department of Chemistry, East Lansing, Michigan 48824, United States*

Complete contact information is available at: https://pubs.acs.org/10.1021/acs.jpcb.3c02803

Notes

The authors declare no competing financial interest.

ACKNOWLEDGMENTS

The research was carried out under the framework of project #W911-NF-14-10063 funded by the Army Research Office. D.K.N.T. was supported by an REU grant from the National Science Foundation (grant CHE-2150173). Any opinions, findings, and conclusions or recommendations expressed in this material are those of the author(s) and do not necessarily reflect the views of the National Science Foundation.

REFERENCES

(1) Wu, C. C.; Wu, C. I.; Sturm, J. C.; Kahn, A. Surface modification of indium tin oxide by plasma treatment: An effective method to improve the efficiency, brightness, and reliability of organic light emitting devices. *Appl. Phys. Lett.* **1997**, *70*, 1348−1350.

(2) Campbell, I. H.; Kress, J. D.; Martin, R. L.; Smith, D. L.; Barashkov, N. N.; Ferraris, J. P. Controlling charge injection in organic electronic devices using self-assembled monolayers. *Appl. Phys. Lett.* **1997**, *71*, 3528−3530.

(3) Morgado, J.; Charas, A.; Barbagallo, N. Reduction of the light-onset voltage of light-emitting diodes based on a soluble poly(p-phenylene vinylene) by grafting polar molecules onto indium−tin oxide. *Appl. Phys. Lett.* **2002**, *81*, 933−935.

(4) Kim, J. S.; Park, J. H.; Lee, J. H.; Jo, J.; Kim, D.-Y.; Cho, K. Control of the electrode work function and active layer morphology via surface modification of indium tin oxide for high efficiency organic photovoltaics. *Appl. Phys. Lett.* **2007**, *91*, No. 112111.

(5) Hanson, E. L.; Guo, J.; Koch, N.; Schwartz, J.; Bernasek, S. L. Advanced Surface Modification of Indium Tin Oxide for Improved Charge Injection in Organic Devices. *J. Am. Chem. Soc.* **2005**, *127*, 10058−10062.

(6) Guo, J.; Koch, N.; Schwartz, J.; Bernasek, S. L. Direct Measurement of Surface Complex Loading and Surface Dipole and Their Effect on Simple Device Behavior. *J. Phys. Chem. B* **2005**, *109*, 3966−3970.

(7) Yu, S.-Y.; Chang, J.-H.; Wang, P.-S.; Wu, C.-I.; Tao, Y.-T. Effect of ITO Surface Modification on the OLED Device Lifetime. *Langmuir* **2014**, *30*, 7369−7376.

(8) Ho, P. K. H.; Granström, M.; Friend, R. H.; Greenham, N. C. Ultrathin Self-Assembled Layers at the ITO Interface to Control Charge Injection and Electroluminescence Efficiency in Polymer Light-Emitting Diodes. *Adv. Mater.* **1998**, *10*, 769−774.

(9) Cui, J.; Huang, Q.; Veinot, J. G. C.; Yan, H.; Marks, T. J. Interfacial Microstructure Function in Organic Light-Emitting Diodes: Assembled Tetraaryldiamine and Copper Phthalocyanine Interlayers. *Adv. Mater.* **2002**, *14*, 565−569.

(10) Yan, H.; Huang, Q.; Cui, J.; Veinot, J. G. C.; Kern, M. M.; Marks, T. J. High-Brightness Blue Light-Emitting Polymer Diodes via Anode Modification Using a Self-Assembled Monolayer. *Adv. Mater.* **2003**, *15*, 835−838.

(11) Appleyard, S. F. J.; Day, S. R.; Pickford, R. D.; Willis, M. R. Organic electroluminescent devices: enhanced carrier injection using SAM derivatized ITO electrodes. *J. Mater. Chem.* **2000**, *10*, 169−173.

(12) Hatton, R. A.; Willis, M. R.; Chesters, M. A.; Rutten, F. J. M.; Briggs, D. Enhanced hole injection in organic light-emitting diodes using a SAM-derivatised ultra-thin gold anode supported on ITO glass. *J. Mater. Chem.* **2003**, *13*, 38−43.

(13) Nüesch, F.; Rotzinger, F.; Si-Ahmed, L.; Zuppiroli, L. Chemical potential shifts at organic device electrodes induced by grafted monolayers. *Chem. Phys. Lett.* **1998**, *288*, 861−867.

(14) Appleyard, S. F. J.; Willis, M. R. Electroluminescence: enhanced injection using ITO electrodes coated with a self assembled monolayer. *Opt. Mater.* **1998**, *9*, 120−124.

(15) Susarova, D. K.; Akkuratov, A. V.; Kukharenko, A. I.; Cholakh, S. O.; Kurmaev, E. Z.; Troshin, P. A. ITO Modification for Efficient Inverted Organic Solar Cells. *Langmuir* **2017**, *33*, 10118−10124.

(16) Paniagua, S. A.; Hotchkiss, P. J.; Jones, S. C.; Marder, S. R.; Mudalige, A.; Marrikar, F. S.; Pemberton, J. E.; Armstrong, N. R. Phosphonic Acid Modification of Indium−Tin Oxide Electrodes: Combined XPS/UPS/Contact Angle Studies. *J. Phys. Chem. C* **2008**, *112*, 7809−7817.

(17) Kim, D.; Lee, A. W. H.; Eastcott, J. I.; Gates, B. D. Modifying the Surface Properties of Indium Tin Oxide with Alcohol-Based Monolayers for Use in Organic Electronics. *ACS Appl. Nano Mater.* **2018**, *1*, 2237−2248.

(18) Peiris, T. A. N.; Senthilarasu, S.; Wijayantha, K. G. U. Enhanced Performance of Flexible Dye-Sensitized Solar Cells: Electrodeposition of $Mg(OH)_2$ on a Nanocrystalline TiO_2 Electrode. *J. Phys. Chem. C* **2012**, *116*, 1211−1218.

(19) Mazur, M.; Blanchard, G. J. Surface Immobilized Optical Probes: Pyrene Molecules Covalently Attached to Silica and Indium-Doped Tin Oxide. *Bioelectrochem* **2005**, *66*, 89−94.

(20) Mazur, M.; Krysinski, P.; Michota-Kaminska, A.; Bukowska, J.; Rogalski, J.; Blanchard, G. J. Immobilization of laccase on gold, silver and indium tin oxide by zirconium-phosphonate-carboxylate (ZPC) coordination chemistry. *Bioelectrochem* **2007**, *71*, 15−22.

(21) Horne, J. C.; Huang, Y.; Liu, G.-Y.; Blanchard, G. J. The Correspondence Between Layer Morphology and Intralayer Excitation Transport in Zirconium-Phosphonate Monolayers. *J. Am. Chem. Soc.* **1999**, *121*, 4419−4426.

(22) Blodgett, K. B. Films built by depositing successive monomolecular layers on a solid surface. *J. Am. Chem. Soc.* **1935**, *57*, 1007−1022.

(23) Blodgett, K. B.; Langmuir, I. Built-up films of barium stearate and their optical properties. *Phys. Rev.* **1937**, *51*, 964−982.

(24) Langmuir, I. The constitution and fundamental properties of solids and liquids. II. Liquids. *J. Am. Chem. Soc.* **1917**, *39*, 1848−1906.

(25) Fanucci, G. E.; Seip, C. T.; Petruska, M. A.; Nixon, C. M.; Ravaine, S.; Talham, D. R. Organic/inorganic Langmuir-Blodgett films based on known layered solids: Divalent and trivalent metal phosphonates. *Thin Solid Films* **1998**, *327−329*, 331−335.

(26) Fanucci, G. E.; Talham, D. R. Langmuir-Blodgett films based on known layered solids: Lanthanide(III) octadecylphosphonate LB films. *Langmuir* **1999**, *15*, 3289−3295.

(27) Seip, C. T.; Granroth, G. E.; Meisel, M. W.; Talham, D. R. Langmuir-Blodgett films of known layered solids: Preparation and structural properties of octadecylphosphonate bilayers with divalent metals and characterization of a magnetic Langmuir-Blodgett film. *J. Am. Chem. Soc.* **1997**, *119*, 7084−7094.

(28) Herath, H. N. K.; MacRae, A. L.; Ugrinov, A.; Morello, G. R.; Parent, A. R. Electrochemical properties of Ru polypyridyl phosphonates. *Eur. J. Inorg. Chem.* **2023**, *26*, No. e202200747.

(29) van der Westhuizen, D.; von Eschwege, K. G.; Conradie, J. Electrochemical data of polypyridine complexes of Ru(II). *Data in Brief* **2019**, *27*, No. 104759.

(30) Martín, M.; Horváth, H.; Sola, E.; Kathó, Á.; Joó, F. Water-Soluble Triisopropylphosphine Complexes of Ruthenium(II): Syn-

thesis, Equilibria, and Acetonitrile Hydration. *Organomet.* **2009**, *28*, 561−566.
(31) Cuartero, M.; Acres, R. G.; Bradley, J.; Jarolimova, Z.; Wang, L.; Bakker, E.; Crespo, G. A.; De Marco, R. Electrochemical Mechanism of Ferrocene-Based Redox Molecules in Thin Film Membrane Electrodes. *Electrochim. Acta* **2017**, *238*, 357−367.
(32) Chen, J.; Ikeda, O.; Aoki, K. Electrode reaction of ferrocene in a nitrobenzene+water emulsion. *J. Electroanal. Chem.* **2001**, *496*, 88−94.
(33) Sohail, M.; De Marco, R.; Jarolímová, Z.; Pawlak, M.; Bakker, E.; He, N.; Latonen, R.-M.; Lindfors, T.; Bobacka, J. Transportation and Accumulation of Redox Active Species at the Buried Interfaces of Plasticized Membrane Electrodes. *Langmuir* **2015**, *31*, 10599−10609.
(34) O'Brien, J. T.; Zeppenfeld, A. C.; Richmond, G. L.; Page, C. J. Fourier-Transform Infrared-Spectroscopy Studies of Hafnium Alkylbis(Phosphonate) Multilayers On Gold - Effects of Alkylbis-(Phosphonate) Chain-Length, Substrate Roughness, and Surface Functionalization On Film Structure and Order. *Langmuir* **1994**, *10*, 4657−4663.
(35) Zeppenfeld, A. C.; Fiddler, S. L.; Ham, W. K.; Klopfenstein, B. J.; Page, C. J. Variation of Layer Spacing in Self-Assembled Hafnium-1,10- Decanediylbis(Phosphonate) Multilayers As Determined By Ellipsometry and Grazing Angle X-Ray-Diffraction. *J. Am. Chem. Soc.* **1994**, *116*, 9158−9165.
(36) Kohli, P.; Rini, M. C.; Major, J. S.; Blanchard, G. J. Elucidating the Balance between Metal Ion Complexation and Polymer Conformation in Maleimide-Vinyl Ether Polymer Multilayer Structures. *J. Mater. Chem.* **2001**, *11*, 2996−3001.
(37) Feldheim, D. L.; Mallouk, T. E. Layer-by-layer assembly and intercalation reactions of iron(III) and iron(II) alkanebisphosphonates on gold surfaces. *Chem. Commun.* **1996**, No. 22, 2591−2592.
(38) Cao, G.; Lee, H.; Lynch, V. M.; Mallouk, T. E. Synthesis and Structural Characterization of a Homologous Series of Divalent-Metal Phosphonates, Mii(O3pr).H2o and Mii(Ho3pr)2. *Inorg. Chem.* **1988**, *27*, 2781−2785.
(39) Cao, G.; Lee, H.; Lynch, V. M.; Mallouk, T. E. Structural Studies of Some New Lamellar Magnesium, Manganese and Calcium Phosphonates. *Solid St. Ion.* **1988**, *26*, 63−69.
(40) Cao, G.; Mallouk, T. E. Shape-Selective Intercalation Reactions of Layered Zinc and Cobalt Phosphonates. *Inorg. Chem.* **1991**, *30*, 1434−1438.
(41) Soumpasis, D. M. Theoretical analysis of fluorescence photobleaching recovery experiments. *Biophys. J.* **1983**, *41*, 95−97.
(42) Sprague, B. L.; Pego, R. L.; Stavreva, D. A.; McNally, J. G. Analysis of binding reactions by fluorescence recovery after photobleaching. *Biophys. J.* **2004**, *86*, 3473−3495.

https://doi.org/10.1021/acs.jpcb.3c02803
J. Phys. Chem. B 2023, 127, 7785−7795